Dynamic Properties of Rubber Vibration Isolators and Antivibration Performance of a Nanoclay-Modified Silicone/Poly(propylene oxide)–Poly(ethylene oxide) Copolymer with 20 wt % $LiClO_4$ Blend System

Hsien-Tang Chiu, Jyh-Horng Wu, Zhi-Jian Shong

Graduate School of Polymer Engineering, National Taiwan University of Science and Technology, 43 Keelung Road, Section 4, Taipei, Taiwan

Received 24 June 2005; accepted 18 September 2005
DOI 10.1002/app.23218
Published online in Wiley InterScience (www.interscience.wiley.com).

ABSTRACT: This research explores the interlayer effect, hysteresis behavior, and dynamic antivibration properties of a poly(propylene oxide)–poly(ethylene oxide) copolymer with 20 wt % $LiClO_4$ (PEL) for modified silicone [silicone/polymer electrolyte (SP)] blends with clay and organoclay in various amounts. The results show that the polymer chains of PEL expand the clay gallery distance from 1.21 to 1.84 nm. Clay, after it has been organically modified, is added to SP blends, and its gallery spacing shortens from 2 to 1.7 nm. From the compression hysteresis results, along with the increased content of unmodified clay, the antivibration performance of the blends is elevated. In the dynamic antivibration testing results, along with the addition of clay and organoclay, the dynamic ratio of the blends is decreased; thus, in the vibration isolation performance, there is evidence of an elevated effect. On the other hand, after the clay is modified with ammonium salt, its vibration isolation effect is not better than that of the unmodified clay. In terms of the formulation of the nanocomposites, when the concentration of the clay is less than 4 wt %, it has a better effect on the vibration isolation and antivibration effect of SP blends. © 2006 Wiley Periodicals, Inc. J Appl Polym Sci 101: 3713–3720, 2006

Key words: clay; nanocomposites; silicones

INTRODUCTION

Polymers used as antivibration materials have been widely used in, for example, machine, transportation, and construction industries. Along with the development of high technology, demands for antivibration materials have been increasing rapidly, particularly for aeronautics, precision instruments, and so forth. Polymers exhibit uniquely high damping behavior in their glass-transition zone because of the conversion of mechanical vibrations into heat energy through friction between molecular chains and heat dissipation.[1] However, this high damping property cannot be maintained with a large variation of the temperature or frequency. Thus, many studies have proposed methods of increasing the damping of polymers in a wide range of temperatures and frequencies,[2–12] such as blending, copolymerization, and interpenetrated networks (IPNs). However, the polymer material's inherent sustaining strength usually cannot satisfy the antivibration structural design. Thus, in the earlier studies of Kerwin,[13] Ungar and Beranek,[14] Weibo and Fengchang,[5] Oborn et al.,[11] and Yamada et al.,[12] a sandwich structure of a polymer/steel laminate was used to increase the stiffness of the polymer damping material. Some research also used blended fillers[5,15–17] and fibers[18–22] in polymers to enhance their stiffness and antivibration performance. The energy-loss mechanisms include friction between polymer chains, friction between polymers and fillers,[1] and interactions between polymer and fibers.

Silicone rubber can be used for extensive applications, and the visible characteristics of silicon rubber include low glass-transition temperatures,[23,24] high impact resistance,[25,26] thermal stability,[27] high mechanical and chemical resistance, weatherproofing, ozone resistance, and radiation resistance.[28,29] It is widely applied in various industrial products. The application of polymer electrolytes is very broad, including solid-state batteries, sensors, and display devices.[30–35] In this investigation, nanoclay was used, and it contained layered silicates with the dimensions of $100 \times 100 \times 1$ nm^3.[36] Isomorphic substitution within the layers generated negative charges that were normally counterbalanced by cations residing in the interlayer galleries space.[37,38]

In our previous research, the linear molecular structure of a liquid polymer electrolyte was entangled in the silicone polymer network structure, forming a semi-IPN and increasing the damping properties.[39]

Correspondence to: H.-T. Chiu (george6916@yahoo.com.tw).

TABLE I
Compositions of the SP/Clay Nanocomposites (wt %)

Material	Clay content (wt %)				Organoclay content (wt %)			
Silicone rubber	88.2	86.4	84.6	82.8	88.2	86.4	84.6	82.8
PEL	9.8	9.6	9.4	9.2	9.8	9.6	9.4	9.2
Clay	2	4	6	8	—	—	—	—
Organoclay	—	—	—	—	2	4	6	8

Also, we explored the curing behavior, intermolecular interactions, and mechanical and thermal properties of clay and organoclay in silicone/polymer electrolyte (SP) blends; the liquid polymer electrolytes were able to intercalate in the clay gallery.[40]

The main goal of this study was to evaluate the effect of the incorporation of layered clay and organoclay into SP blends in forming intercalated nanocomposites via blending with random nanoscale sandwich structure dampers having high stiffness and antivibration properties. In our experiments, the variation of the basal plane spacing of clay and organoclay in the SP blends was investigated with X-rays; hysteresis phenomenon and dynamic property tests were conducted to evaluate the antivibration performance and vibration isolation of the polymer material to evaluate the effect of the *d*-spacing of the nanoclay on the SP blending system.

EXPERIMENTAL

Materials

The materials included liquid silicone (polydimethylsiloxane; model 9050), hydrogen-functional siloxane oligomers (used as curing agents and manufactured by Dow Corning), a poly(propylene oxide)–poly(ethylene oxide) copolymer with 20 wt % $LiClO_4$ (PEL; used as a liquid polymer electrolyte and manufactured by Japan Carlit, Tokyo, Japan), Na^+-nontronite (clay; model PK805; obtained from Pai Kong Nanotechnology Co., Ltd.), and hexadecyldimethylethyl ammonium bromide (CTAB; purchased from Acros, Somerville, NJ).

Preparation of the organoclay

n-Hexadecyltrimethyl ammonium bromide (4.2 g; intercalative reagent) was dissolved in 250 mL of distilled water with vigorous stirring to form a uniformly dispersed solution. Then, 5 g of Na^+-nontronite was added to the solution, which was stirred for 24 h, filtered, and then washed three times with 400 mL of hot water to remove NaBr. After being washed with ethanol (250 mL) to remove residual ammonium salt, the modified clay was dried in a vacuum oven at 80°C for 24 h.

Preparation of the specimen

The sample for testing was mixed in the proportions specified in Table I. It was produced by the mixing of clay and organoclay in PEL, before stirring with silicone, and then placed in a mold. The mold was maintained at 150°C for 200 min of curing. After cooling, the test piece was removed from the mold and trimmed to the proper size for testing.

X-ray measurements

Wide-angle X-ray diffraction experiments were conducted on a Rigaku D/Max RC X-ray diffractometer with Cu Kα radiation (λ = 1.5418 A) at 40 kV and 100 mA with a scanning rate of 2°/min.

Mechanical property measurements

The tensile strength and elongation at break were measured with a universal tensile tester with a tension velocity of 500 mm/min in compliance with the specifications of ASTM D 412C.

Determination of the compression stiffness (k_s)

A material testing system (MTS-810) was used to test k_s of the test piece with dimensions of 40 ± 0.5 mm × 40 ± 0.5 mm ×12 ± 0.5 mm under a deformation range of 2 mm:[39]

$$k_s = F/X \tag{1}$$

where F is the compression force and X is the compression displacement.

Determination of the compression hysteresis

The measurements were carried out with a materials testing system (MTS-810) at a frequency of 1 Hz and an amplitude of 2 mm. The loss of energy in each cycle (ΔW) was calculated from the hysteresis loop, and the damping constant (β) was calculated from ΔW as follows:[41]

$$\Delta W = \pi K \beta X^2 \tag{2}$$

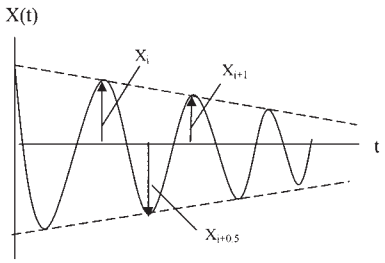

Figure 1 Typical hysteresis damping curve.

where K is the stiffness of the material and X is the displacement (mm). The calculated β value was then converted into the hysteresis damping curve. X is the amplitude of the part in the ith cycle, X_i, $X_{i+0.5}$, and X_{i+1} represents the number of vibration wave (similar to Figure 1):[41]

$$\frac{X_i}{X_{i+0.5}} = \sqrt{\frac{2+\pi\beta}{2-\pi\beta}} \tag{3}$$

$$\frac{X_{i+0.5}}{X_{i+1}} = \sqrt{\frac{2+\pi\beta}{2-\pi\beta}} \tag{4}$$

Testing methods for the dynamic properties of vibration isolation

The SRIS 3503-1990[42] nonresonance testing method was employed: the specimens were placed in a material testing system (MTS-810) and subjected to vibrations at a frequency of 1 Hz and an amplitude of 2 mm. Figure 2 presents a loading–amplitude graph under a sine wave loading, with the horizontal axis being the amplitude and the vertical axis being the loading. The energy loss of the nanocomposites (ΔW) is the area surrounded by the loading–amplitude curve. W is the rectangle area, P is the load, P_0 is the half load, X is the amplitude, X_0 is the half amplitude, $|k^*|$ is the absolute resilience modulus, δ is the phase angle, k_1 is the storage modulus, k_2 is the loss modulus, c is the damping coefficient, ω is the angular

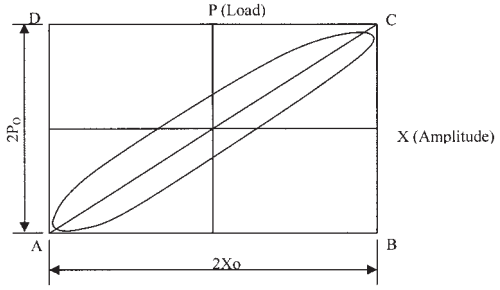

Figure 2 State of a load–displacement curve.

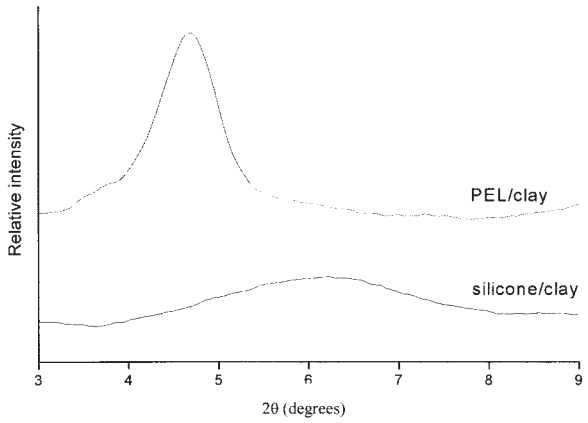

Figure 3 XRD patterns of silicone/clay and PEL/clay nanocomposites.

frequency, tan δ (the damping or loss factor) is k_2/k_1, and R is the dynamic ratio:[42]

$$|k^*| = P_o/X_o = BC/AB \tag{5}$$

$$\sin\delta = (2/\pi) \times (\Delta W/W) \tag{6}$$

$$k_1 = |k^*|\cos\delta \tag{7}$$

$$k_2 = |k^*|\sin\delta \tag{8}$$

$$c = k_2/\omega \tag{9}$$

$$\tan\delta = k_2/k_1 \tag{10}$$

$$R = |k^*|/k_s \tag{11}$$

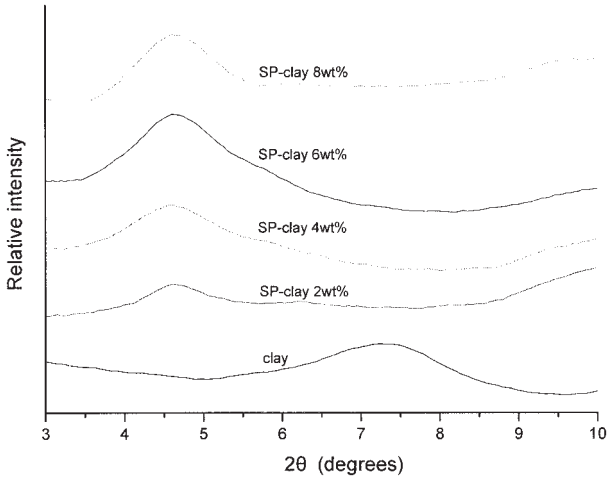

Figure 4 XRD patterns of SP/clay nanocomposites containing various clay concentrations (wt %).

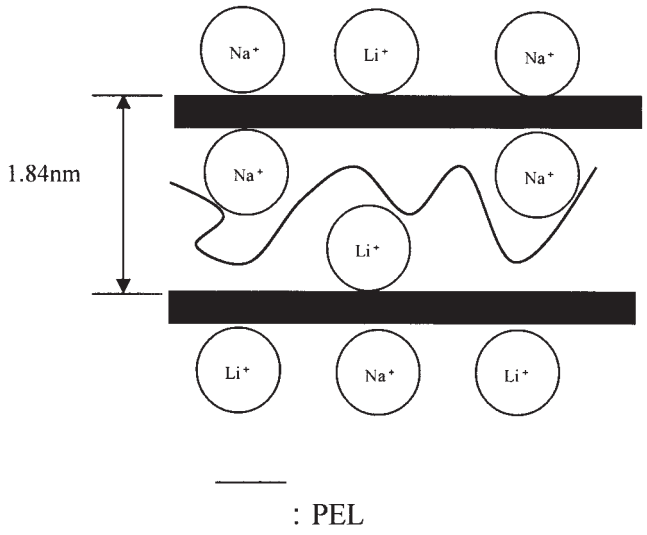

Figure 5 Structure of the SP/clay nanocomposites.

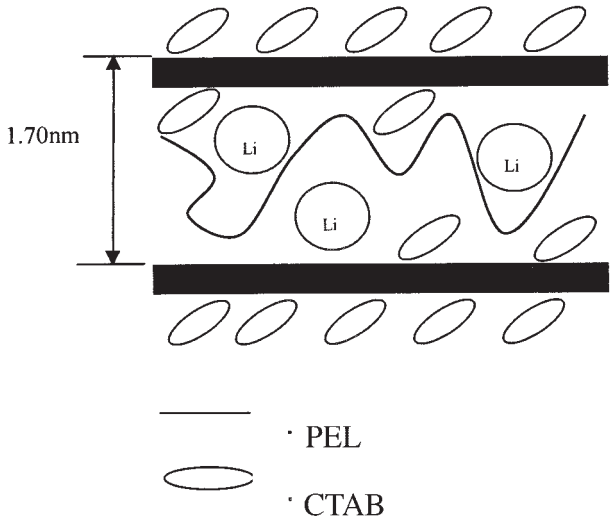

Figure 7 Structure of the SP/organoclay nanocomposites.

RESULTS AND DISCUSSION

Influence on the basal plane space of the SP/clay nanocomposites

The surface of clay can attract positive ions,[37,38] which cause clay to be hydrophilic. Organic polymer chains, mostly consisting of hydrocarbons, are hydrophobic. Each polymer chains is so large that it cannot easily enter the clay gallery from intercalated composites.[43] Therefore, this experiment mainly used CTAB as the surfactant, which had an ion exchange with the Na^+ ions of the clay and produced ion bonds. The bulky alkyl ammonium molecules formed larger interlayer spacing. The modified clay was hydrophobic with a lower surface energy and was more compatible with organic polymers. The effect of the organic modifiers on the intercalating behavior of the polymer could also be confirmed from an XRD pattern. As expected, the intercalation of the polymer chains further increased the interlayer spacing of the clay over that of the pure clay, shifting the diffraction peak toward lower θ values.

Cheng[44] reported poly(ethylene oxide) (PEO)/clay nanocomposites when the clay was not organically modified. The basal interlayer spacing increased from 1.24 to 1.78 nm. Nevertheless, the diffraction peak was not obviously shifted by a variation of the clay content in the PEO/clay hybrid. When the clay was treated organically in the PEO polymer with 2.9% organic clay, the basal interlayer spacing increased. However, the basal interlayer spacing appeared at higher clay contents (>5.7%), and this diffraction peak shifted toward a higher angle as the clay concentration increased; this indicating a lower interlayer spacing between the silicate layers. This phenomenon can be attributed to fewer polymer chains intercalating

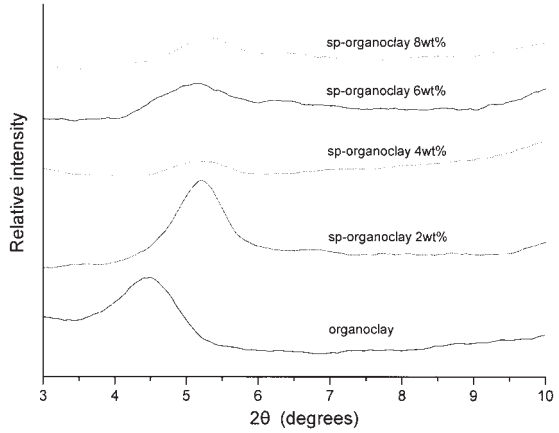

Figure 6 XRD patterns of SP/organoclay nanocomposites containing various organoclay concentrations (wt %).

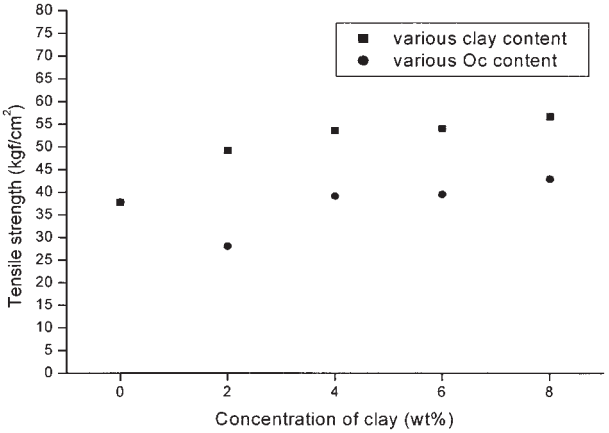

Figure 8 Tensile strength of SP blends with various clay and organically modified clay contents.

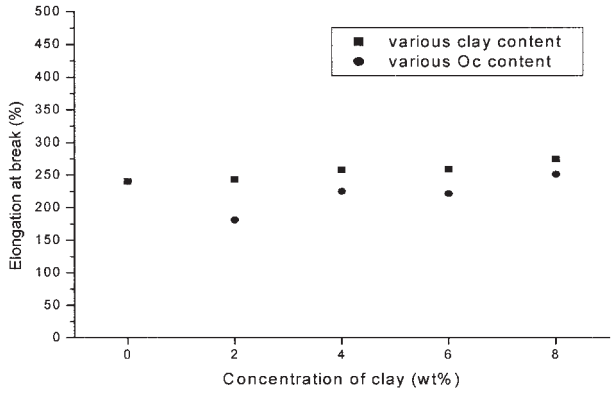

Figure 9 Elongation at break of SP blends with different clay and organically modified clay contents.

within the clay galleries.[44] Adding more hydrophilic clay increased the hydrophilicity and reduced the compatibility between the clay and the hydrophobic polymer; this increased agglomeration among these clay layers.[44]

Figure 3 presents the X-ray patterns of silicone/clay and PEL/clay with broad diffraction peaks. The basal spacing of the clay was 1.21 nm ($2\theta = 7.3°$). The diffraction peak of the silicone/clay deviated from the original $2\theta = 7.3°$ to a lower scattering angle location of $2\theta = 6.2°$ and a PEL/clay scattering angle location of $2\theta = 4.9$. At this time, the interlayer spacing expanded to 1.42 and 1.88 nm. This indicated that the compatibility of PEL with clay was better than that of the silicone.

Figure 4 presents the X-ray pattern of SP blends with various clay contents with broad diffraction peaks. After clay was mixed into an SP blend, the diffraction peak deviated from the original $2\theta = 7.3°$ to a lower scattering angle location of $2\theta = 4.8°$. At this time, the interlayer spacing expanded to 1.84 nm (Fig. 5), and this showed that the PEL polymer chains intercalated within the clay galleries.

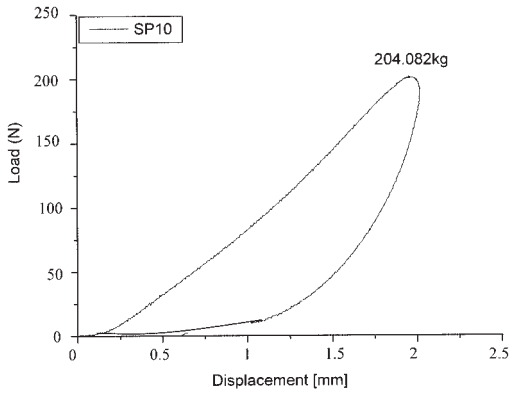

Figure 10 Hysteresis loops of SP blends (the compression loading was 55 kg, the frequency was 1 Hz, and the amplitude was 2 mm).

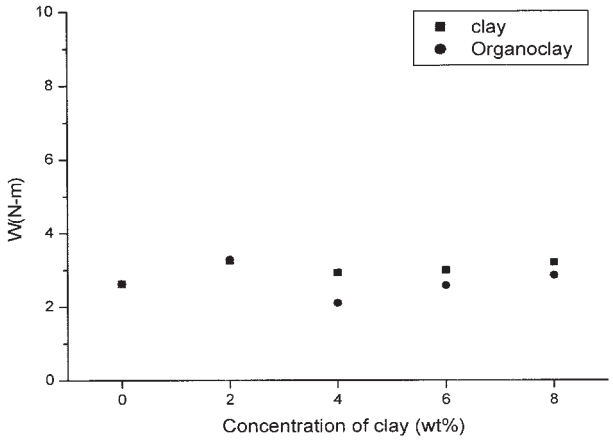

Figure 11 ΔW (N m) of SP/clay hybrids containing various clay and organoclay contents.

Figure 6 presents the X-ray patterns of SP blends with various organoclay contents with broad diffraction peaks. The diffraction peak of the organoclay deviated from the original $2\theta = 7.3°$ to a lower scattering angle location of $2\theta = 4.4°$. At this time, the basal spacing expanded to 2 nm, and this showed that CTAB and the sodium ions of the clay gallery had an effective ion exchange, which successfully intercalated into the galleries of the clay. Theoretically, the organoclay offered a greater chance for the PEL polymer to enter clay gallery, expanding the gallery spacing and evenly distributing itself among the PEL polymer chains. However, the figure shows that the diffraction peak of the organoclay, after it was initially mixed with PEL and added to silicone, moved from the original $2\theta = 4.4°$ to a higher scattering angle location of $2\theta = 5.2°$. At this time, the interlay spacing was 1.70 nm (Fig. 7). This phenomenon can be attributed to the PEL polymer chains, which caused CTAB of the clay galleries to be squeezed out. Therefore, it reduced the compatibility between the clay and the SP blends and

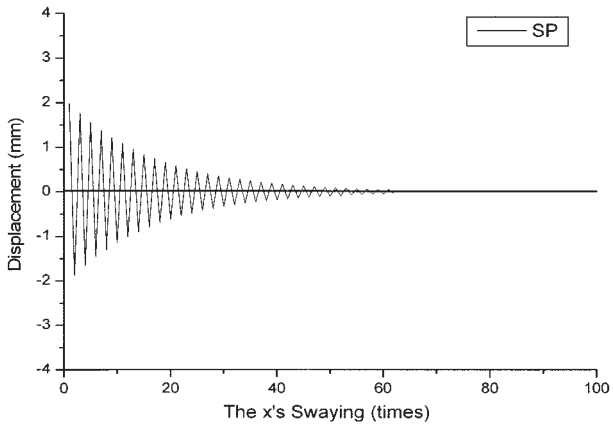

Figure 12 Hysteresis damping curves of SP blends.

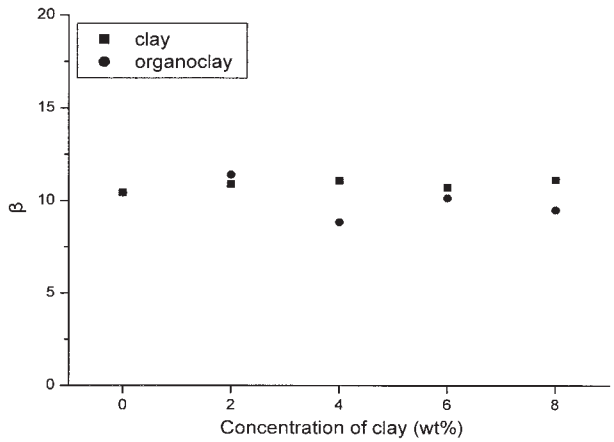

Figure 13 β of SP/clay hybrids containing various clay and organoclay contents.

consequently hindered the entry of polymer chains into the clay galleries and collapsed the originally widened organoclay gallery spacing by 0.3 nm.[40]

Mechanical property analysis of SP/clay nanocomposites

Figures 8 and 9 show the tensile strength and elongation at break curves of clay and organoclay with different contents with the addition of SP blends. The tensile strength and elongation at break of the unmodified clay with the addition of SP blends were better than those of the SP/organoclay nanocomposite system. Along with the increased content of clay and organoclay (4–8 wt %), the tensile strength of the SP blends was elevated, and the elongation characteristics of the SP blends were maintained. Moreover, when the organoclay concentration was less than 2 wt %, the tensile strength was reduced. This phenomenon could be seen in the previous X-ray experiment; the ammonium salt was squeezed by the PEL polymer and then absorbed in the clay layer surface, creating a plastic effect and thereby causing the tensile strength of the SP blends to decrease.[40] When the concentration of the organoclay was increased to 4–8 wt %, the amount of absorbed ammonium salts was increased, the interaction effect between the silicone and clay was increased, and thus the tensile strength was increased correspondingly.

Hysteresis of the SP/clay nanocomposites

Under alternating stress, hysteresis occurs when the rate of deformation lags behind the rate of stress variation. In this case, because the energies absorbed and released are not balanced in each cycle, the stretching and recoil curves form a closed loop known as a hysteresis loop. The area of the loop represents the energy loss. For rubber materials, a larger hysteresis loop means higher damping, which can reduce vibration.[45]

Figure 10 shows the hysteresis loop of SP under compressive vibration at 20°C, 1 Hz, and an amplitude of 2 mm. ΔW[41] may be obtained from the hysteresis loops. Figure 11 shows that the antivibration performance of the SP blends was increased with an increase in the clay content. When ammonium salts modified the clay at a concentration of 4–8 wt %, the antivibration performance of the SP blends could not be increased. Thus, ammonium salts affected the antivibration performance of the SP/organoclay nanocomposites.

Polymer materials have viscous and elastic properties and hence exhibit hysteresis under the action of an external force. The β values may be derived from the area surrounded by hysteresis loops. According to the theory of free vibration, the vibration isolation of materials can be evaluated from β and the hysteresis damping characteristics.[41]

Figure 12 shows the vibration–damping curve of the SP blends. The β values derived from the hysteresis loops are shown in Figure 13, which indicates the β value of SP (10.441). With a higher β value and hence greater viscosity factor, SP energy dissipated faster at certain amplitudes and reached stability with less vibration. With a 2–8 wt % concentration for the

TABLE II
Dynamic Properties of the Antivibration Performance of the SP/Clay Nanocomposites

		Clay content (wt %)				Organoclay content (wt %)			
	SP	2	4	6	8	2	4	6	8
$\lvert k^* \rvert$	102.04	121.02	107.24	113.36	116.93	116.83	96.58	103.21	121.99
δ	11.817	12.6	12.78	11.78	12.53	12.62	9.91	11.33	11.66
k_1	100.28	118.65	105.08	111.43	114.67	114.54	95.41	101.57	119.94
k_2	18.83	23.79	21.396	20.86	22.88	23.01	14.98	18.31	22.23
c	2.997	3.780	3.405	3.320	3.642	3.662	2.38	2.91	3.539
k_s	55.835	40.228	54.884	55.189	38.226	48.249	55.046	57.896	58.695
tan δ	0.188	0.20	0.204	0.187	0.200	0.201	0.157	0.180	0.185
R	3.655	3.008	1.954	2.054	3.059	2.422	1.755	1.783	2.078

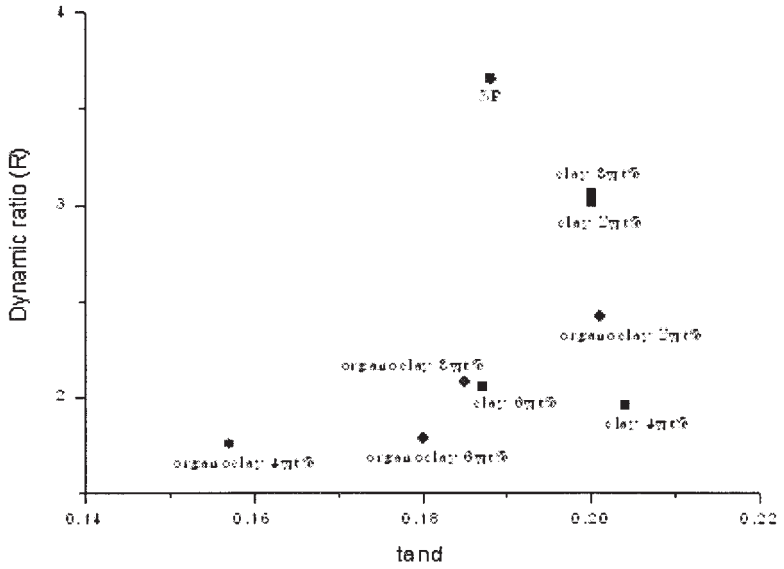

Figure 14 *R* and tan δ of SP/clay hybrids with various clay and organoclay contents.

SP blend clay mixture, its β value was elevated to 10.712–11.118, and the SP/clay nanocomposites were vibrated; the oscillation amplitude stopped the vibration after a short period. This shows that the clay is beneficial to the vibration isolation performance of SP blends. When ammonium salts modified the clay, at organoclay concentrations greater than 2 wt %, the vibration isolation performance of the SP blends could not be increased. This shows that the presence of excessive amounts of ammonium salts is detrimental to the vibration isolation performance of SP/organoclay nanocomposites. These phenomena and Figure 11 show similar trends. Therefore, ammonium salts play an important role in the design of materials in terms of their vibration isolation and antivibration performance.

Dynamic properties of the SP/clay nanocomposite vibration isolation and antivibration

The relationship of *R* and tan δ may be used to evaluate the antivibration and vibration isolation effects of the rubber material. Table II depicts dynamic testing results of SP supplemented with clay or organoclay under a loading of 20 kg at 20°C, 1 Hz, and an amplitude of 2 mm. With lower *R*, there is a better antivibration effect; and a greater tan δ value is favorable to shock absorption. The relationship of *R* and tan δ is depicted in Figure 14. As for vibration isolation, SP blends added to clay and organoclay can raise the vibration isolation performance. Moreover, the vibration isolation effect of clay modified with ammonium salts is not much better than that of unmodified clay. Thus, the presence of ammonium salts is beneficial to the vibration isolation performance of SP/organoclay nanocomposites, and there is a trend in which with the elevation of the vibration isolation effect, the antivibration performance is lowered. As for the antivibration performance, the unmodified clay, below a concentration of 4 wt %, has a better effect on the antivibration performance of SP blends. Moreover, below a 4–8 wt % concentration of the organoclay, because of the influence of ammonium salts, the antivibration nature of an SP blend cannot be raised. Figure 15 shows a damping coefficient curve line drawing of different contents of the clay and organoclay with the incorporation of SP blends. It shows a trend of the antivibration performance of SP blends similar to that of Figure 14. In terms of the formulation of the nanocomposites, a clay concentration of 4 wt % has a better

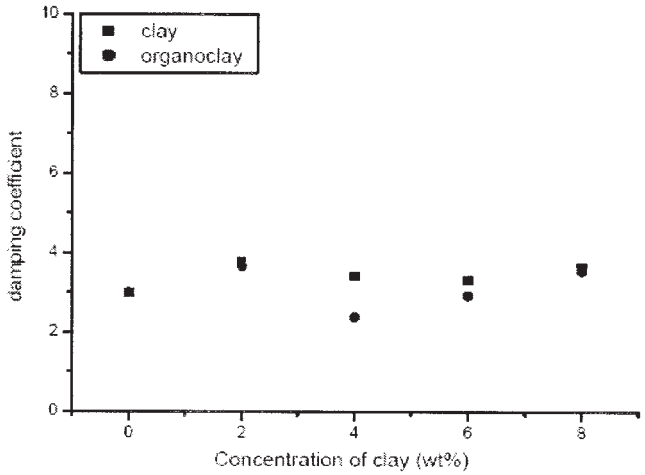

Figure 15 Damping coefficient of SP/clay hybrids containing various clay and organoclay contents.

effect on the vibration isolation and antivibration performance of the SP blends.

CONCLUSIONS

The X-ray results of SP blends with clay treated by swelling agents show that the swelling agent in the clay layers is squeezed out by PEL and adsorbed to the clay surface, and the clay maintains its layered structure intact and scatters in the polymer to form interlayered nanocomposites. A compressive vibration hysteresis study indicates that the area of the hysteresis loop increases with an increasing content of organically modified clay; that is, the antivibration performance is better. In a relational curve of R and tan δ, the blends containing 6–10 wt % clay exhibit higher tan δ values and lower R values, which suggest that the addition of clay gives the SP blends better antivibration and vibration isolation effects.

References

1. Hur, T.; Mason, J. A.; Sperling, L. H. J Polym Sci Part B: Polym Phys 1989, 27, 2251.
2. Sha'aban, A. K.; McCartney, S.; Patel, N.; Yilgor, I.; Riffle, J. S.; Dwight, D. W.; McGrath, J. E. Polym Prep 1983, 24, 130.
3. Hartmann, B. Polym News 1991, 16, 134.
4. Manson, J. A.; Sperling, L. H. Polymer Blends and Composites; Plenum: New York, 1976.
5. Weibo, H.; Fengchang, Z. J Appl Polym Sci 1993, 50, 277.
6. Mathew, A.; Chakraborty, B. C.; Deb, P. C. J Appl Polym Sci 1994, 53, 1107.
7. Tung, C. J.; Hsu, T. C. J. J Appl Polym Sci 1992, 46, 1759.
8. Chen, Q.; Ge, H.; Chen, D.; He, X.; Yu, X. J Appl Polym Sci 1994, 54, 1191.
9. Chang, M. C. O.; Thomas, D. A.; Sperling, L. H. J Appl Polym Sci 1987, 34, 409.
10. Foster, J. N.; Sperling, L. H. J Appl Polym Sci 1987, 33, 2637.
11. Oborn, J.; Bertilsson, H.; Rigdahl, M. J Appl Polym Sci 2001, 80, 2865.
12. Yamada, W.; Shoji, S.; Sasakl, H.; Nagatanl, A.; Yamaguchi, K.; Kohjiya, S.; Hashim, A. S. J Appl Polym Sci 1999, 71, 855.
13. Kerwin, E. M. J Acoust Soc Am 1959, 31, 952.
14. Ugar, E. E.; Beranek, L. L. Noise and Vibration Control; McGraw-Hill: New York, 1971.
15. Law, H. H.; Rossiter, P. L.; Koss, L. L.; Simon, G. P. J Mater Sci 1995, 30, 2648.
16. Kwak, G. H.; Inoue, K.; Tominaga, Y.; Asal, S.; Sumita, M. J Appl Polym Sci 2001, 82, 3058.
17. Wong, D. T. H.; Williams, H. L. J Appl Polym Sci 1983, 28, 2187.
18. Yarlagadda, S.; Lesieutre, G. J Spacecraft Rockets 1995, 12, 825.
19. Asams, R. D.; Maheri, M. R. J Alloys Compd 2003, 355, 126.
20. Saravanos, D. A.; Chamis, C. C. J Compos Technol Res 1990, 12, 31.
21. Gu, W.; Kampe, S. L.; Lu, G. Q.; Wu, H. F. J Mater Sci 1998, 33, 5731.
22. Chiu, H. T.; Chiu, S. H.; Wu, J. H.; Ger, G. S. J Mater Sci Eng 2001, 33, 200.
23. Ohiberg, S. M.; Alexander, L. E.; Warrick, E. L. J Polym Sci 1958, 27, 1.
24. Polmantee, K. E.; Hunter, M. J. J Appl Polym Sci 1959, 1, 3.
25. Hagerman, E. M. J Appl Polym Sci 1969, 13, 1873.
26. Matsuo, M.; Kondo, Y. Polym Eng Sci 1970, 10, 253.
27. Polmanteer, K. E. Rubber Chem Technol 1981, 54, 1051.
28. Eaborn, C. Organosilicon Compounds; Butterworths: London, 1962.
29. Noll, W. Chemistry and Technology of Siloxanes; Academic: New York, 1968.
30. Chiang, C. K. Polym Commun 1981, 22, 1454.
31. Hooper, A.; North, J. M. Solid State Ionics 1983, 9, 1161.
32. Gauthier, M.; Fauteux, D.; Vassort, G.; Belanger, A.; Duval, M.; Ricoux, P.; Chabagno, J. M.; Muller, D.; Rigaud, P.; Armand, M. B.; Deroo, D. J Appl Polym Sci 1985, 132, 1333.
33. Skotheim, T. A.; Inganas, O. J Electrochem Soc 1985, 132, 2116.
34. Abraham, K. M.; Alamgir, M.; Perrotti, S. J. J Electrochem Soc 1988, 135, 535.
35. West, K.; Christiansen, B. Z.; Jacobsen, T.; Atlung, S. J Electrochem Soc 1985, 132, 3061.
36. Akelah, A.; Moet, A. J Appl Polym Sci Appl Polym Symp 1994, 55, 153.
37. Giannelis, E. P. Adv Mater 1996, 8, 29.
38. Alexandre, M.; Dubois, P. Mater Sci Eng 2000, 28, 1.
39. Chiu, H. T.; Wu, J. H. J Appl Polym Sci, to appear.
40. Chiu, H. T.; Wu, J. H. J Polym Res 2004, 11, 247.
41. Rao, S. S. Mechanical Vibrations; 2nd ed., Addison-Wesley: New York, 1990.
42. SRIS 3503 J Soc Rubber Ind 1990, 63, 233.
43. Pinnavaia, T. J.; Bell, G. W.; Scheirs, J. Polymer–Clay Nanocomposites; Wiley: Chichester, England, 2000.
44. Cheng, H. W.; Chiu, C. Y.; Chang, F. C. J Polym Sci Part B: Polym Phys 2002, 40, 1342.
45. Sperling, L. H. Introduction to Physical Polymer Science, 2nd ed.; Wiley: New York, 1992.